Modulation-based superradiant phase transition in the strong-coupling regime

Jin-Feng Huang[1,2,*] and Lin Tian[2,†]

[1]*Key Laboratory of Low-Dimensional Quantum Structures and Quantum Control of Ministry of Education, Key Laboratory for Matter Microstructure and Function of Hunan Province, Department of Physics and Synergetic Innovation Center for Quantum Effects and Applications, Hunan Normal University, Changsha 410081, China*

[2]*School of Natural Sciences, University of California, Merced, California 95343, USA*

(Received 26 August 2022; revised 13 April 2023; accepted 8 June 2023; published 28 June 2023)

The Dicke model can exhibit quantum phase transition between the normal and the superradiant phases when the strength of the light-matter coupling exceeds the ultrastrong-coupling regime. However, it is challenging to observe this phase transition in practical systems due to limited coupling strength or finite two-photon A^2 terms. Here we show that by applying a periodic modulation to the frequency of the two-level systems in a standard Dicke model in the strong-coupling regime, an anisotropic Dicke model with tunable rotating and counter-rotating terms in the ultrastrong-coupling regime can be achieved. We calculate the ground state and the excitation spectrum of this model in terms of the modulation parameters. Our result shows that the superradiant phases can be observed in cavity- or circuit-quantum electrodynamics systems with strong coupling.

DOI: 10.1103/PhysRevA.107.063713

I. INTRODUCTION

The Dicke model [1] describes a cavity mode coupled to multiple quantum two-level systems (or qubits) in cavity- or circuit-quantum electrodynamics (QED) systems [2–7]. It has been widely studied to exhibit the superradiant phase transition at a critical temperature or a critical light-matter coupling strength [8–15], where the superradiant phase is characterized by macroscopic excitations of the cavity and the qubits. At zero temperature, a quantum phase transition (QPT) between the normal and the superradiant phases can occur when the coupling strength exceeds the ultrastrong-coupling regime. Dynamical phase transition has been studied both theoretically and experimentally in dissipative Dicke models [16–22]. Recently, it was shown that the Dicke model can be simulated with four-level atoms via cavity-assisted Raman transitions, and nonequilibrium phase transition has been demonstrated experimentally in this system [23,24].

Despite intensive efforts with both atomic systems and solid-state devices, it is still challenging to observe the ground-state superradiant phase transition in the Dicke model due to limited coupling strength or the two-photon A^2 term in some systems. For atomic systems in the ultrastrong-coupling regime, the A^2 terms resulted from second-order effects of the light-matter interaction can prevent the occurrence of the superradiant phase transition [25,26]. Note that the Dicke phase transition and the symmetry-breaking phases can be demonstrated with motional degrees of freedom of Bose-Einstein condensates coupled to a cavity mode [3,5]. In the superconducting circuit-QED systems, although the ultrastrong-coupling regime can now be reached [27–31], imperfection of the quantum circuits could affect the behavior of this phase transition, as was studied in Ref. [32] using a mean-field approach.

In this work, we present an approach that enables the observation of the quantum superradiant phase transition in a standard Dicke model in the strong-coupling regime with the strength of the collective light-matter coupling much smaller than qubit and cavity frequencies. In our approach, by applying a periodic modulation to the frequency of the qubits in the standard Dicke model, a tunable anisotropic Dicke model with ultrastrong rotating and counter-rotating couplings can be generated. The qubit frequency modulation generates sidebands in the energy spectrum of the qubits. By adjusting the frequency and magnitude of the modulation in the anisotropic Dicke model, it is possible to tune the ratio of coupling strengths between the dominant rotating and counter-rotating sidebands relative to the effective frequencies of the qubits and the cavity over a broad range. Both the rotating and the counter-rotating terms can reach the ultrastrong-coupling regime. With the collective qubit-cavity couplings in the strong-coupling regime compared to the original qubit and cavity frequencies, the strength of the two-photon A^2 terms is also much smaller than these frequencies. The A^2 terms can hence be safely neglected as they are far off resonance in our scheme. This makes it possible to observe the superradiant phase in the cavity-QED setup, which was considered impossible in previous works [25,26]. We calculate the ground-state phases and excitation spectra vs the modulation parameters. Our result shows that ground state superradiant phases can be observed in the cavity- or circuit-QED systems in the strong-coupling regime. Given the tunability of the effective model in this approach, it can be utilized to study phase transitions in related models such as the Tavis-Cummings model [33] and

*Corresponding author: jfhuang@hunnu.edu.cn
†Corresponding author: ltian@ucmerced.edu

the Lipkin-Meshkov-Glick model [34]. Our work can inspire future studies on implementing quantum phase transitions in engineered quantum systems.

II. MODEL

Consider a standard Dicke model, where a cavity mode is coupled to N qubits with the frequency of the qubits periodically modulated. The total Hamiltonian has the form $H_t = H_{\rm SD} + H_{A^2} + H_{\rm M}(t)$, which includes the Hamiltonian of the standard Dicke model ($\hbar \equiv 1$)

$$H_{\rm SD} = \omega_0 J_z + \omega_c a^\dagger a + g_0 N^{-1/2}(J_+ + J_-)(a + a^\dagger), \quad (1)$$

a two-photon A^2 term $H_{A^2} = g_{A^2}(a + a^\dagger)^2$ with amplitude g_{A^2}, and a periodic modulation of the qubit frequency $H_{\rm M}(t) = \xi\nu\cos(\nu t)J_z$ with dimensionless driving magnitude ξ and modulation frequency ν. Here $J_z = \sum_{i=1}^N \sigma_z^{(i)}/2$ and $J_\pm = \sum_{i=1}^N \sigma_\pm^{(i)}$ are collective spin operators defined as the sum of the Pauli operators $\sigma_{z,\pm}^{(i)}$ of the qubits, ω_0 is the energy splitting of the qubits, a ($a^\dagger$) is the annihilation (creation) operator and ω_c the frequency of the cavity mode, and $g_0/\sqrt{N}$ is the coupling strength between an individual qubit and the cavity mode. The collective spin operators obey the usual angular momentum commutation relations $[J_z, J_\pm] = \pm J_\pm$ and $[J_+, J_-] = 2J_z$, and have the angular momentum eigenstates $|j, m\rangle$ with maximum eigenvalue $j_{\max} = N/2$ and $m \in [-j,\ j]$.

The standard Dicke model can exhibit quantum phase transition from a normal phase to a superradiant phase with macroscopic cavity displacement and qubit excitations. This phase transition occurs when the collective coupling strength reaches the ultrastrong-coupling regime with $g_0 \geqslant \sqrt{\omega_0\omega_c}/2$ [1,13]. The amplitude of the two-photon Hamiltonian H_{A^2} can be written as $g_{A^2} = \chi g_0^2/\omega_0$, with χ being a dimensionless coefficient. In cavity QED, governed by the Thomas-Reiche-Kuhn sum rule, $\chi \geqslant 1$, which prevents the occurrence of the superradiant phase transition [26]. Even though we can have $\chi \ll 1$ in circuit QED, other factors such as the parameter spread of the qubits in the ultrastrong-coupling regime could prevent the observation of this phase transition.

Below we derive the effective Hamiltonian of the standard Dicke model under periodic modulation using the approach in Ref. [35]. Let $H_0^{(1)} = \omega_0 J_z + \omega_c' a^\dagger a + H_{\rm M}(t)$ with $\omega_c' = \omega_c + 2g_{A^2}$, which includes the modulation of the qubit frequency. In the rotating frame of $H_0^{(1)}$, the effective Hamiltonian of the modulated Dicke model is $H_{\rm rot}^{(1)} = V_1^\dagger(t)(H_{\rm t} - H_0^{(1)})V_1(t)$ with $V_1(t) = \exp[-i\int_0^t H_0^{(1)}(\tau)d\tau]$. After omitting the constant term in H_{A^2}, we find that

$$H_{\rm rot}^{(1)} = \frac{g_0}{\sqrt{N}}\sum_{n=-\infty}^{\infty} J_n(\xi)[J_+(ae^{i\delta_n t} + a^\dagger e^{i\Delta_n t}) + \text{H.c.}] + g_{A^2}(a^2 e^{-2i\omega_c' t} + a^{\dagger 2}e^{2i\omega_c' t}), \quad (2)$$

where $\delta_n = \omega_0 - \omega_c' + n\nu$, $\Delta_n = \omega_0 + \omega_c' + n\nu$, and J_n is the nth Bessel function of the first kind with integer number n. Here we have used the Jacobi-Anger identity: $\exp[i\xi\sin(\nu t)] = \sum_{n=-\infty}^{\infty} J_n(\xi)\exp(in\nu t)$ for Bessel functions. As shown in Eq. (2), the modulation of the qubit frequency generates spectral sidebands in the rotating (counter-rotating) terms with detuning δ_n (Δ_n) and coupling amplitude $(g_0/\sqrt{N})J_n(\xi)$. The sidebands are separated by the modulation frequency ν. The amplitudes of the sidebands can be adjusted by varying the dimensionless modulation amplitude ξ.

We introduce a second rotating frame defined by the Hamiltonian $H_0^{(2)} = -\tilde{\omega}_0 J_z - \tilde{\omega}_c a^\dagger a$ with the effective qubit and cavity frequencies $\tilde{\omega}_0 = (\delta_{n_0} + \Delta_{m_0})/2$ and $\tilde{\omega}_c = (\Delta_{m_0} - \delta_{n_0})/2$, respectively. Here by choosing appropriate qubit frequency and modulation frequency, we can select a rotating sideband n_0 and a counter-rotating sideband m_0, where the effective coupling $\lambda_r = g_0 J_{n_0}(\xi)$ [$\lambda_{\rm cr} = g_0 J_{m_0}(\xi)$] for the sideband can reach the ultrastrong-coupling regime with respect to its rotating frequency $|\delta_{n_0}|$ ($|\Delta_{m_0}|$). Meanwhile, under the condition $\omega_0, \omega_c, \nu \gg g_0$, all other sidebands are fast rotating, i.e.,

$$g_0|J_{n\neq n_0}(\xi)|,\ g_0|J_{m\neq m_0}(\xi)| \ll \nu, |\delta_{n\neq n_0}|, |\Delta_{m\neq m_0}|. \quad (3)$$

With $g_0 \ll \omega_0$, $g_{A^2} \ll g_0$ and $g_{A^2} \ll 2\omega_c'$. The a^2 and $a^{\dagger 2}$ terms with oscillating frequencies $\pm 2\omega_c'$ from the two-photon A^2 Hamiltonian are hence also fast rotating (see Appendix A). In the rotating frame of $H_0^{(2)}$, the effective Hamiltonian is $H_{\rm rot}^{(2)} = V_2^\dagger(t)(H_{\rm rot}^{(1)} - H_0^{(2)})V_2(t)$ with the unitary transformation $V_2(t) = \exp[-iH_0^{(2)}t]$. Under the rotating-wave approximation with all fast-rotating sidebands of $n \neq n_0$ and $m \neq m_0$ and the two-photon A^2 terms neglected, the Hamiltonian becomes

$$H_{\rm rot}^{(2)} = \tilde{\omega}_0 J_z + \tilde{\omega}_c a^\dagger a + N^{-1/2}[J_+(\lambda_r a + \lambda_{cr} a^\dagger) + \text{H.c.}]. \quad (4)$$

This Hamiltonian describes an anisotropic Dicke Hamiltonian with tunable frequencies $\tilde{\omega}_0(\nu)$ and $\tilde{\omega}_c(\nu)$ that depend on the modulation frequency ν and with effective couplings $\lambda_r(\xi)$ and $\lambda_{cr}(\xi)$ for the rotating and the counter-rotating terms, respectively, that depend on the dimensionless modulation amplitude ξ.

III. ULTRASTRONG COUPLING

The parameters in Eq. (4) can be adjusted to reach the ultrastrong-coupling regime by varying the frequency ν and the amplitude ξ of the periodic modulation. We define $\lambda^C = \sqrt{\tilde{\omega}_0\tilde{\omega}_c}$ as the critical coupling, which is crucial for our discussion of the superradiant phase transition and only depends on the driving frequency ν. In Fig. 1(a), we plot λ^C/ω_0 vs ν/ω_0. At $\omega_0 = \omega_c'$, the index for the rotating sideband is $n_0 = 0$ with $\delta_{n_0} = 0$, whereas the index m_0 for the counter-rotating sideband varies with ν/ω_0 and reaches $m_0 = 0$ when $\nu > 2(\omega_0 + \omega_c')$. It can be shown that $\lambda^C = 0$ at $\nu = -2\omega_0/m_0$ or $\nu = -2\omega_c'/m_0$, for a given value of m_0. For $\omega_0 = \omega_c'$, the curve of λ^C/ω_0 is hence composed of V-shaped valleys when $\nu < 2(\omega_0 + \omega_c')$. Each valley shares the same value of m_0 with the minima of the valleys being at $\nu = -2\omega_0/m_0$, respectively. Thus, the minima of the V-shaped valleys of the critical coupling strength λ^C form an harmonic sequence towards $\nu = 0$.

The effective coupling strengths depend on the driving amplitude ξ in the form of the Bessel functions. In Figs. 1(b) and

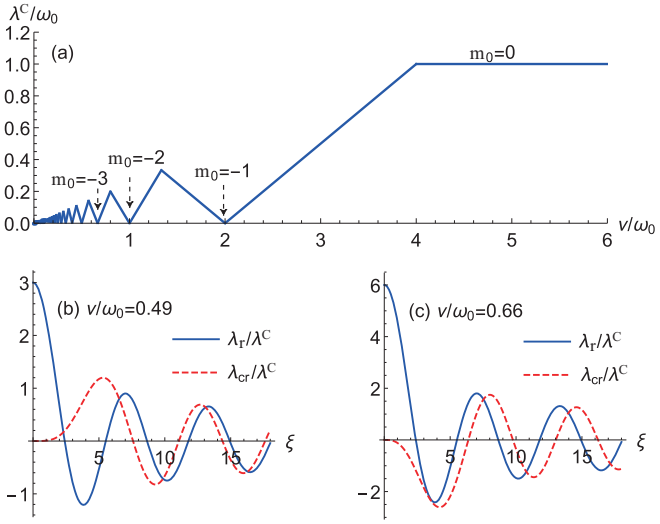

FIG. 1. (a) The ratio λ^C/ω_0 between the critical coupling and the qubit frequency vs the relative modulation frequency ν/ω_0. (b and c) The ratios λ_r/λ^C and λ_{cr}/λ^C vs the driving amplitude ξ for $g_0/\omega_0 = 0.06$ at $\nu/\omega_0 = 0.49$ and 0.66, respectively. Here we choose $\omega_0 = \omega_c' = 1$ as the energy unit, and ξ is the dimensionless driving amplitude.

1(c), we plot $\lambda_r(\xi)/\lambda^C$ and $\lambda_{cr}(\xi)/\lambda^C$ vs ξ at $g_0 = 0.06\omega_0$, $\omega_0 = \omega_c'$ for two values of the driving frequency ν. For $\nu/\omega_0 = 0.49$, $n_0 = 0$ and $m_0 = -4$. As ξ increases, $\lambda_r(\xi)/\lambda^C$ oscillates smoothly between 3 and -1.208 with reducing amplitude, and $\lambda_{cr}(\xi)/\lambda^C$ oscillates between 1.199 and -0.823. Both couplings can be tuned to zero when the corresponding Bessel function becomes zero. For $\nu/\omega_0 = 0.66$, $n_0 = 0$ and $m_0 = -3$, and $\lambda_r(\xi)$ and $\lambda_{cr}(\xi)$ exhibit similar behavior. This result shows that both $\lambda_r(\xi)$ and $\lambda_{cr}(\xi)$ can be tuned in a broad range and can enter the ultrastrong-coupling regime. In particular, in the neighborhood of the valley dips in Fig. 1(a), these couplings can exceed the magnitude of the critical coupling λ^C. Our system can hence demonstrate rich quantum phenomena as discussed below.

IV. QUANTUM PHASE TRANSITION

In the Holstein-Primakoff representation, the collective angular momentum operators can be written as $J_+ = b^\dagger\sqrt{N - b^\dagger b}$, $J_- = \sqrt{N - b^\dagger b}\, b$, and $J_z = b^\dagger b - N/2$ [36] in terms of a bosonic mode with annihilation (creation) operator b ($b^\dagger$) and $[b, b^\dagger] = 1$. The anisotropic Dicke model in (4) then becomes

$$H_{\rm rot}^{(2)} = \tilde{\omega}_0 b^\dagger b + \tilde{\omega}_c a^\dagger a - N\tilde{\omega}_0/2 + [b^\dagger\sqrt{1 - b^\dagger b/N}(\lambda_r a + \lambda_{cr} a^\dagger) + \text{H.c.}]. \quad (5)$$

The ground state of the anisotropic Dicke model can be either in a normal phase with $\langle a\rangle = \langle b\rangle = 0$ or in a superradiant phase with finite $\langle a\rangle$ and $\langle b\rangle$, depending on the coupling strengths λ_r and λ_{cr}. To derive the ground state, we use a mean-field approach [8–10,13] and write the bosonic operators as $a \to c + \alpha$ and $b \to d + \beta$, where $\alpha = \langle a\rangle$ ($\beta = \langle b\rangle$) is the semiclassical displacement of the cavity (collective qubit mode), and operator c (d) represents the quantum fluctuation of the displaced cavity (qubit) mode with $\langle c\rangle = 0$ ($\langle d\rangle = 0$). Denote $\vec{v}_S = (c, d, c^\dagger, d^\dagger)^T$. In the thermodynamic limit $N \to \infty$, using a Taylor expansion of the Hamiltonian $H_{\rm rot}^{(2)}$ in terms of the fluctuation operators c and d and keeping to the second-order terms, we have $H_{\rm rot}^{(2)} = H_{II} + H_I + E_G$, where $H_{II} = \vec{v}_S^\dagger G \vec{v}_S$ with G being a 4×4 Hermitian matrix, $H_I = \vec{\Omega}^T\vec{v}_S$ with $\vec{\Omega}$ being a 4×1 vector, and $E_{\rm G}$ is a constant. Here the matrix G, vector $\vec{\Omega}$, and E_G all depend on the displacements α and β, details of which can be found in Appendix B. When α and β correspond to the ground-state displacements, the linear term disappears with $H_I = 0$. Hence, by solving the equation $\vec{\Omega} = 0$, we can find the solution to the semiclassical displacements α and β and derive the ground-state energy E_G and the matrix G.

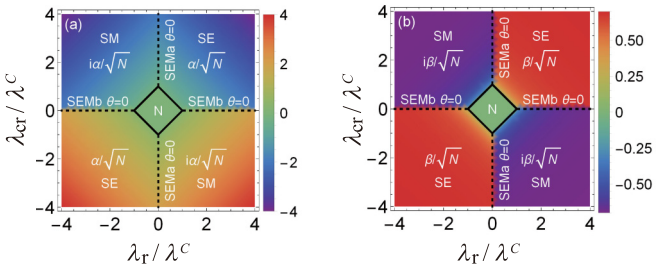

FIG. 2. The dimensionless displacements (a) $\alpha/\sqrt{N}$ (or $i\alpha/\sqrt{N}$) and (b) $\beta/\sqrt{N}$ (or $i\beta/\sqrt{N}$) vs the couplings λ_r/λ^C and λ_{cr}/λ^C. In the SEMa and SEMb phases, we choose $\theta = 0$. Other parameters are $\nu/\omega_0 = 0.49$, $g_0/\omega_0 = 0.06$, and $\omega_0 = \omega_c' = 1$.

The displacements of the cavity and qubit modes in the anisotropic Dicke model are plotted in Figs. 2(a) and 2(b). When $|\lambda_{cr} \pm \lambda_r| < \lambda^C$, $\alpha = \beta = 0$, which corresponds to the normal phase as labeled by N in Fig. 2. Outside the normal phase, when $\lambda_r\lambda_{cr} > 0$, the ground state is in the superradiant electric (SE) phase with two sets of solutions $(\alpha, \beta) = \pm(\alpha_0, \beta_0)$ and α_0, β_0 being real numbers. When $\lambda_r\lambda_{cr} < 0$, the ground state is in the superradiant magnetic (SM) phase with two sets of imaginary number displacements $\pm(i\alpha_0, i\beta_0)$. Along the y axis when $|\lambda_{cr}| > \lambda^C$, the system is in the superradiant electromagnetic a (SEMa) phase, where the semiclassical displacements are $(\alpha_0 e^{-i\theta}, \beta_0 e^{i\theta})$ with an arbitrary but opposite phase factor θ. Similarly, along the x axis when $|\lambda_r| > \lambda^C$, the system is in the superradiant electromagnetic b (SEMb) phase with displacements $(\alpha_0 e^{i\theta}, \beta_0 e^{i\theta})$. Details of these solutions can be found in Appendix B. The solutions in the SE and SM phases break the Z_2 symmetry of the model when $\lambda_r\lambda_{cr} \neq 0$, whereas the solutions in the SEMa and SEMb phases break the U(1) symmetry of the model when $\lambda_r\lambda_{cr} = 0$. Note that for $\lambda_r = \lambda_{cr}$, the condition for the normal phase becomes $|\lambda_r| < \lambda^C/2$, which agrees with the result for a standard Dicke model [9]. The solid and the dashed lines in Fig. 2 indicate the phase boundaries separating these phases. Using the Hopfield-Bogoliubov transformation on H_{II} [37], the system Hamiltonian can be diagonalized as $H_{\rm rot}^{(2)} = \sum_{i=\pm}\omega_i^p \gamma_i^{p\dagger}\gamma_i^p + E_G^p$. Here γ_i^p ($\gamma_i^{p\dagger}$) is the annihilation (creation) operator of one of the quasiparticles in the ground state phase p with frequency ω_i^p, and E_G^p is the ground-state energy in phase p. The operator γ_i^p is a linear combination of the operators $c, c^\dagger, d, d^\dagger$ for the superradiant

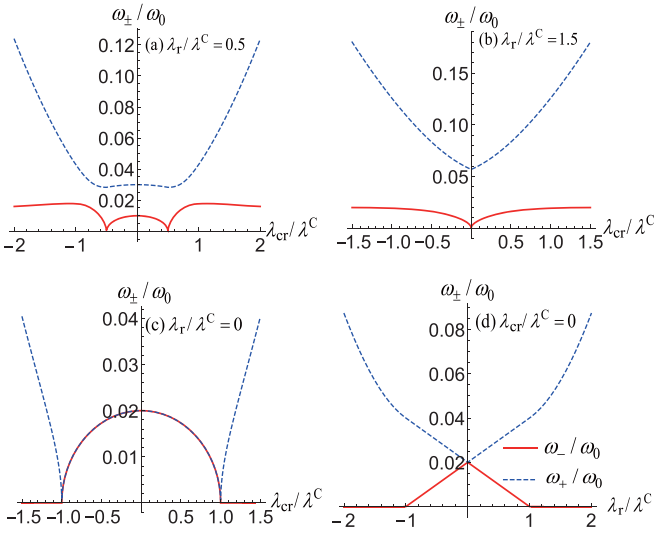

FIG. 3. (a)–(c) The relative quasiparticle spectrum $\omega_\pm/\omega_0$ vs the relative coupling λ_{cr}/λ^C at $\lambda_r/\lambda^C = 0.5, 1.5, 0$, respectively. (d) $\omega_\pm/\omega_0$ vs the relative coupling λ_r/λ^C at $\lambda_{cr}/\lambda^C = 0$. Other parameters are the same as those in Fig. 2.

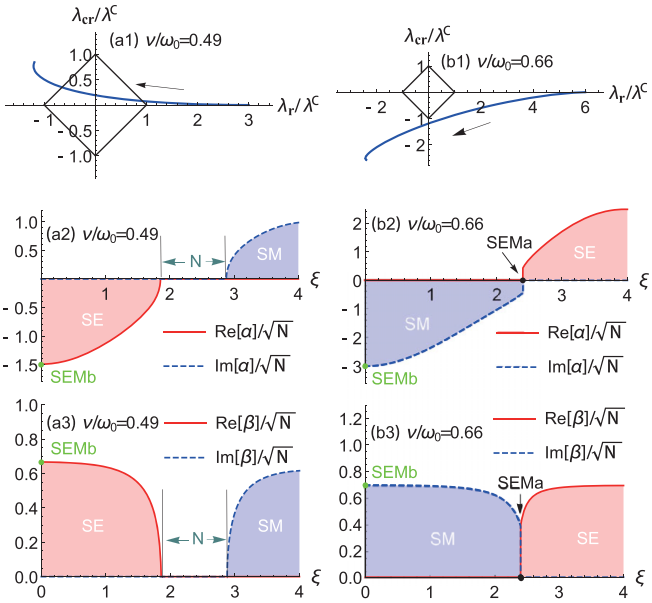

FIG. 4. (a1, b1) The parametrized curves of the relative couplings $[\lambda_r(\xi)/\lambda^C, \lambda_{cr}(\xi)/\lambda^C]$ when the dimensionless driving amplitude ξ increases from 0 to 4 as indicated by the arrows. (a2, b2) The displacement $\alpha/\sqrt{N}$ and (a3, b3) the displacement $\beta/\sqrt{N}$ vs the driving amplitude ξ. (a1)–(a3) are for $\nu/\omega_0 = 0.49$ and $m_0 = -4$. (b1)–(b3) are for $\nu/\omega_0 = 0.66$ and $m_0 = -3$. For SEMa and SEMb phases, we set $\theta = 0$. Other parameters are the same as in Figs. 1(b) and 1(c).

phases and $a, a^\dagger, b, b^\dagger$ for the normal phase, with the commutation relation $[\gamma_i^p,\ \gamma_j^{p\dagger}] = \delta_{ij}$. Details of the quasiparticle spectrum for different phases are given in Appendix C. In Fig. 3, we plot the quasiparticle spectrum as functions of the coupling λ_{cr} or λ_r. The superscript "p" that refers to the specific phase in the quasiparticle frequency is omitted. For $\lambda_r/\lambda^C = 0.5$, the critical points occur at $\lambda_{cr}/\lambda^C = \pm 0.5$ when $\omega_- = 0$, as shown in Fig. 3(a). The system experiences a second-order phase transition from the normal phase at $|\lambda_{cr}/\lambda^C| < 0.5$ to the SE or SM phase at $|\lambda_{cr}/\lambda^C| > 0.5$, as shown in Fig. 2. For $\lambda_r/\lambda^C = 1.5$ presented in Fig. 3(b), a single critical point occurs at $\lambda_{cr}/\lambda^C = 0$, which corresponds to a Goldstone mode in the SEMb phase [10]. For $\lambda_r/\lambda^C = 0$ along the y axis, the critical points are at $\lambda_{cr}/\lambda^C = \pm 1$, corresponding to a phase transition between the normal phase and the SEMa phase, as shown in Fig. 3(c). Similarly, for $\lambda_{cr}/\lambda^C = 0$ along the x axis, the normal-SEMb phase transition occurs at $\lambda_r/\lambda^C = \pm 1$, as shown in Fig. 3(d). In both the SEMa and SEMb phases, $\omega_- = 0$, corresponding to Goldstone excitations resulted from the U(1) symmetry of the model along the x and y axes.

V. MANIPULATION OF QUANTUM PHASES

By controlling the parameters of the qubit frequency modulation, the effective rotating and counter-rotating couplings in the engineered anisotropic Dicke model can reach the ultrastrong-coupling regime with superradiant ground states, even if the physical coupling strength is only in the strong-coupling regime. In particular, as shown in Fig. 1(a), the critical coupling $\lambda^C \to 0$ in the neighborhood of a V-shaped minimum, which results in diminishing normal phase region.

In Figs. 4(a1) and 4(b1), we plot the parametrized curves of the effective couplings $[\lambda_r(\xi)/\lambda^C, \lambda_{cr}(\xi)/\lambda^C]$ vs the driving amplitude ξ at $\nu/\omega_0 = 0.49$ and 0.66, respectively. It can be seen that the parametrized curves evolve through several superradiant phases and the normal phase. In Figs. 4(a2), 4(a3), 4(b2), and 4(b3), we plot the ground-state displacements α and β vs ξ for the corresponding values of ν/ω_0. As labeled in the plots, the solid curves are for the real parts and the dashed curves are for the imaginary parts of α and β. We also indicate the corresponding ground-state phases in the plots. At $\nu/\omega_0 = 0.49$ in Figs. 4(a2) and 4(a3), the ground state is in the SE phase when $0 < \xi < 1.856$, where $\lambda_r(\xi)\lambda_{cr}(\xi) > 0$ and $|\lambda_r(\xi) + \lambda_{cr}(\xi)| > \lambda^C$. In the region $2.880 < \xi < 4$, the ground state is in the SM phase with $\lambda_r(\xi)\lambda_{cr}(\xi) < 0$ and $|\lambda_r(\xi) - \lambda_{cr}(\xi)| > \lambda^C$. The SEMb phase with $\lambda_{cr}(\xi) = 0$ is located at $\xi = 0$. The normal phase appears when $1.856 < \xi < 2.880$. Here the dependence of $\lambda_r(\xi)/\lambda^C, \lambda_{cr}(\xi)/\lambda^C$ vs ξ can be seen in Fig. 1(b). At $\nu/\omega_0 = 0.66$ with the increase of ξ, the ground state is in the SEMb, SM, SEMa, and SE phases sequentially, as shown in Figs. 4(b2) and 4(b3). The dependence of $\lambda_r(\xi)/\lambda^C, \lambda_{cr}(\xi)/\lambda^C$ vs ξ can be found in Fig. 1(c). With these two values of ν/ω_0, all normal and superradiant phases can be experienced.

The above result shows that the ground state of the engineered anisotropic Dicke model can be in a superradiant phase when the collective qubit-cavity coupling is only in the strong-coupling regime with, e.g., $g_0/\omega_0 = 0.06$. For superconducting qubits with $\omega_0/2\pi = 10$ GHz, this corresponds to $g_0/2\pi = 600$ MHz with a single qubit-cavity coupling of $g_0/\sqrt{N}$. With only $N = 4$ qubits, the single qubit-cavity coupling is 300 MHz, well within reach of current technology [38,39]. In comparison, the ground state of the standard Dicke model can be in the superradiant phase only when $g_0/\omega_0 >$

0.5 in the ultrastrong-coupling regime. This requires a collective coupling of $g_0/2\pi = 5$ GHz. Even if the individual qubit-cavity coupling can reach 1 GHz, it would require an array of $N = 25$ qubits to achieve such collective coupling. Qubit frequencies can be modulated with various approaches. For superconducting qubits, frequency modulation can be achieved with a tunable junction (or SQUID), where the effective Josephson energy (and hence qubit frequency) can be tuned by applying oscillating magnetic field to the SQUID loop. For atomic qubits formed by hyperfine states in atoms or ions, qubit frequency can be modulated via Zeeman effect by applying oscillating magnetic field. For the parameter $\nu/\omega_0 = 0.49$ (0.66) used in our work, the modulation frequency $\nu/2\pi = 4.9$ (6.6) GHz, and the modulation amplitude $\xi\nu/2\pi$ is in the range of (0, 19.6) [(0, 26.4)] GHz with $0 < \xi < 4$. These modulation parameters are achievable in experiments. Note that the phase transition studied in this work is for the ground states in a rotating frame under the frequency modulation. The normal and the superradiant phases can be prepared using an adiabatic approach. Without the frequency modulation, the superconducting qubit-cavity system can be prepared to their ground state, which is in a normal phase with no excitation, by cooling down the system under cryogenic temperature (e.g., 20 mK in a dilution fridge). Then by slowly turning on the modulation amplitude ξ to the desired value, the system can reach the superradiant phase adiabatically with high probability [5,40,41]. Our result hence shows that the normal-superradiant phase transition can be implemented with practical physical systems in the strong-coupling regime. Meanwhile, various superradiant phases such as SE, SM, SEMa, and SEMb phases can all be reached by varying the modulation parameters. By manipulating these parameters, one can demonstrate rich physics in different superradiant phases, such as the Goldstone modes in the SEMa and SEMb phases.

The phase transition studied above focuses on the regime of negligible cavity dissipation with $\kappa/\omega_0, \kappa/\omega_c' < 10^{-4}$, where κ is the cavity dissipation rate. The parameter ranges discussed above satisfy the requirement of negligible dissipation. Meanwhile, when the cavity dissipation becomes non-negligible, the effective anisotropic Dicke Hamiltonian generated with our approach can also be used to study steady-state phase transition. As shown in Refs. [2,11], the critical coupling strength for the superradiant phase transition in the presence of a finite cavity dissipation becomes $\lambda_{\rm dis}^C = \frac{1}{2}\sqrt{\tilde{\omega}_0(\kappa^2 + \tilde{\omega}_c^2)/\tilde{\omega}_c}$. Consider a dissipation rate of $\kappa = 0.02\omega_0$. At $\nu/\omega_0 = 0.49$ (0.66), $\kappa \sim \tilde{\omega}_0$, $\tilde{\omega}_c$, and $\lambda_{\rm dis}^C = 0.707\lambda^C$ ($1.118\lambda^C$), which is comparable to λ^C. The effective coupling strengths in the engineered anisotropic Dicke model can hence be stronger than $\lambda_{\rm dis}^C$ under our parameters, and the steady-state superradiant phase can be reached.

VI. CONCLUSIONS

We studied a scheme that can generate an anisotropic Dicke model with ultrastrong coupling via classical control of engineered quantum systems. By applying properly designed qubit frequency modulation to a standard Dicke model in the strong-coupling regime, the effective rotating and counter-rotating couplings can be tuned in a broad range and reach the ultrastrong-coupling regime. We show that various superradiant phases and the normal phase can be achieved in the ground state of this anisotropic Dicke model. Our result demonstrates that superradiant phases can be implemented in practical physical systems with a collective light-matter coupling in the strong-coupling regime, and the normal-superradiant phase transition can be observed. With our parameters, the two-photon A^2 terms that could prevent the implementation of the superradiant phases only have negligible effect on the engineered Hamiltonian.

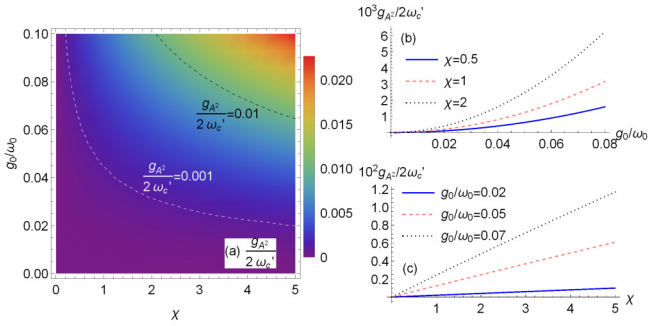

FIG. 5. (a) The ratio $g_{A^2}/2\omega_c'$ vs the relative qubit-cavity coupling g_0/ω_0 and the dimensionless factor χ. (b) $10^3 g_{A^2}/2\omega_c'$ vs g_0/ω_0 at selected values of χ. (c) $10^2 g_{A^2}/2\omega_c'$ vs χ at selected values of g_0/ω_0. Here $\omega_0 = \omega_c$.

ACKNOWLEDGMENTS

J.-F.H. is supported in part by the National Natural Science Foundation of China (Grant No. 12075083) and the Natural Science Foundation of Hunan Province, China (Grant No. 2020JJ5345). L.T. is supported by the NSF awards (Grants No. 2006076 and No. 2037987) and the UCOP-MRPI Program (Grant ID M23PL5936).

APPENDIX A: TWO-PHOTON A^2 TERM

The two-photon (A^2) terms are given by the Hamiltonian $H_{A^2} = g_{A^2}(a + a^\dagger)^2$ with amplitude $g_{A^2} = \chi g_0^2/\omega_0$ and χ being a dimensionless coefficient. In our discussion, the $a^\dagger a$ term in H_{A^2} has been absorbed into the Hamiltonian of the standard Dicke model by replacing the cavity frequency ω_c with the modified frequency $\omega_c' = \omega_c + 2g_{A^2}$. The remaining terms can be written as $g_{A^2}(a^2 + a^{\dagger 2})$. Here we will show that in the strong-coupling limit with $g_0 \ll \omega_0, \omega_c'$, these two terms can be omitted. To justify the validity of this omission and estimate the influence of the omitted terms, we consider the ratio $g_{A^2}/2\omega_c'$. In Fig. 5(a), we plot the ratio $g_{A^2}/2\omega_c'$ vs the collective coupling strength g_0 and the dimensionless factor χ. Our result shows that $g_{A^2}/2\omega_c'$ increases quadratically with g_0 and linearly with χ, which is clearly demonstrated by Figs. 5(b) and 5(c), respectively. However, to reach $g_{A^2}/2\omega_c' = 0.01$, we need to have ($g_0/\omega_0 \sim 0.065$, $\chi \sim 5$) or ($g_0/\omega_0 \sim 0.1$, $\chi \sim 2$), as indicated by the dashed curve in Fig. 5(a). For the parameters of interest in our discussions with $g_0/\omega_0 \sim 0.06$ and $\chi < 0.1$, this ratio is very small with $g_{A^2}/2\omega_c' \ll 0.001$. Hence, it is appropriate to omit these terms from the subsequent discussions.

APPENDIX B: SEMICLASSICAL DISPLACEMENTS α AND β

The Hamiltonian of the anisotropic Dicke model in the Holstein-Primakoff representation is

$$H_{\rm rot}^{(2)} = \tilde{\omega}_0 b^\dagger b + \tilde{\omega}_c a^\dagger a + \left[b^\dagger \sqrt{1 - \frac{b^\dagger b}{N}} (\lambda_r a + \lambda_{cr} a^\dagger) + \text{H.c.} \right] - \frac{N}{2}\tilde{\omega}_0, \tag{B1}$$

i.e., Eq. (5) in the main paper. To solve the ground-state phases, we use a mean-field approach and write the bosonic operators as

$$a \to c + \alpha, \quad b \to d + \beta, \tag{B2}$$

with semiclassical displacement α of the cavity mode and semiclassical displacement β of the collective qubit mode. Define the operator vector $\vec{v}_S = (c, d, c^\dagger, d^\dagger)^T$. In the thermodynamic limit $N \to \infty$, using a Taylor expansion of the Hamiltonian $H_{\rm rot}^{(2)}$ in terms of the fluctuation operators c and d and keeping to the second-order terms, the Hamiltonian then becomes $H_{\rm rot}^{(2)} = H_{II} + H_I + E_G$ with $H_{II} = \vec{v}_S^\dagger G \vec{v}_S$, $H_I = \vec{\Omega}^T \vec{v}_S$, and constant E_G. The matrix G, vector $\vec{\Omega}$, and E_G all depend on the semiclassical displacements α and β. The constant E_G is the energy of the system at the displacements α and β. By minimizing E_G, which is equivalent to letting $\vec{\Omega}^T = 0$ (i.e., $H_I = 0$), we can find the solutions of α and β for the ground state at given system parameters. Then using the Hopfield-Bogoliubov transformation on H_{II}, we can obtain the quasiparticle modes for the corresponding ground state. Below we give the solution to the semiclassical displacements in the ground states of all possible phases.

1. Normal phase

In the normal phase, the semiclassical displacements are $\alpha = \beta = 0$ without macroscopic excitations in the system. Hence, the fluctuation operators $c = a$ and $d = b$. The second-order Hamiltonian is simply

$$H_{\rm rot}^{(2)} = \tilde{\omega}_0 b^\dagger b + \tilde{\omega}_c a^\dagger a + [b^\dagger(\lambda_r a + \lambda_{cr} a^\dagger) + \text{H.c.}] - \frac{N}{2}\tilde{\omega}_0, \tag{B3}$$

which includes second-order contributions in terms of the operators a, $a^\dagger$, b, $b^\dagger$ and the constant term $-N\tilde{\omega}_0/2$.

2. Superradiant phases

In the superradiant phases, the semiclassical displacements are macroscopic with $\alpha, \beta \sim O(\sqrt{N})$. The ground-state energy can be written as

$$E_G = \tilde{\omega}_0 |\beta|^2 + \tilde{\omega}_c |\alpha|^2 + \sqrt{\frac{k}{N}} [\beta^*(\lambda_r \alpha + \lambda_{cr} \alpha^*) + \text{H.c.}] - \frac{N}{2}\tilde{\omega}_0. \tag{B4}$$

The 4×4 matrix G is given by

$$G = \frac{1}{2} \begin{pmatrix} \tilde{\omega}_c & \sqrt{\frac{k}{N}} u_4^* & 0 & \sqrt{\frac{k}{N}} u_5 \\ \sqrt{\frac{k}{N}} u_4 & \tilde{\omega}_d' & \sqrt{\frac{k}{N}} u_5 & -\frac{1}{k}\sqrt{\frac{k}{N}} u_6 \\ 0 & \sqrt{\frac{k}{N}} u_5^* & \tilde{\omega}_c & \sqrt{\frac{k}{N}} u_4 \\ \sqrt{\frac{k}{N}} u_5^* & -\frac{1}{k}\sqrt{\frac{k}{N}} u_6^* & \sqrt{\frac{k}{N}} u_4^* & \tilde{\omega}_d' \end{pmatrix}, \tag{B5}$$

where $k \equiv N - |\beta|^2$,

$$u_1 = \lambda_r \alpha + \lambda_{cr} \alpha^*, \tag{B6a}$$

$$u_2 = \beta \lambda_r + \beta^* \lambda_{cr}, \tag{B6b}$$

$$u_3 = \frac{\beta^* u_1 + \beta u_1^*}{4k}, \tag{B6c}$$

$$u_4 = \lambda_r - \frac{1}{2k}\beta u_2^*, \tag{B6d}$$

$$u_5 = \lambda_{cr} - \frac{1}{2k}\beta u_2, \tag{B6e}$$

$$u_6 = \beta(u_1 + u_3 \beta), \tag{B6f}$$

and $\tilde{\omega}_d' \equiv \tilde{\omega}_0 - \frac{1}{k}\sqrt{\frac{k}{N}} u_3 (4k + |\beta|^2)$. Here, to write H_{II} in matrix form, the constant term $-(\tilde{\omega}_0 + \tilde{\omega}_c)/2 + 2u_3\sqrt{k/N}$ is neglected from H_{II}. The components of the vector $\vec{\Omega}$ are

$$\Omega_c = \tilde{\omega}_c \alpha^* + \sqrt{\frac{k}{N}} (\beta^* \lambda_r + \beta \lambda_{cr}), \tag{B7a}$$

$$\Omega_d = \tilde{\omega}_0 \beta^* + \sqrt{\frac{k}{N}} (\lambda_r \alpha^* + \lambda_{cr} \alpha) - \frac{1}{2k}\sqrt{\frac{k}{N}} \left[|\beta|^2 (\lambda_r \alpha^* + \lambda_{cr} \alpha) + \beta^{*2} (\lambda_r \alpha + \lambda_{cr} \alpha^*) \right]. \tag{B7b}$$

a. SE phase

The ground state of the anisotropic Dicke model is the SE phase when $|\lambda_r + \lambda_{cr}| > \lambda^C$ and $\lambda_r \lambda_{cr} > 0$. The SE phase has two sets of real-number solutions $(\alpha, \beta) = \pm(\alpha_0, \beta_0)$ with

$$\alpha_0 = -(\lambda_r + \lambda_{cr}) \sqrt{N\left(1 - \mu_E^2\right)/2\tilde{\omega}_c}, \tag{B8a}$$

$$\beta_0 = \sqrt{N(1 - \mu_E)/2}, \tag{B8b}$$

where $\mu_E = [\lambda^C/(\lambda_r + \lambda_{cr})]^2$. The corresponding second-order Hamiltonian can be obtained as

$$H_{\rm rot}^{(2)} = \tilde{\omega}_0 \frac{1 + \mu_E}{2\mu_E} d^\dagger d + \tilde{\omega}_c c^\dagger c + \sqrt{\frac{(1 + \mu_E)}{2}} [d^\dagger (\lambda_r c + \lambda_{cr} c^\dagger) + d(\lambda_r c^\dagger + \lambda_{cr} c)] - \frac{(1 - \mu_E)(\lambda_r + \lambda_{cr})}{2\sqrt{2(1 + \mu_E)}} (d^\dagger + d)(c + c^\dagger) + \tilde{\omega}_0 \frac{(1 - \mu_E)}{(1 + \mu_E)} \frac{(3 + \mu_E)}{8\mu_E} (d^\dagger + d)^2 + E_G, \tag{B9}$$

which will be used to derive the quasiparticle modes in Appendix C.

b. SM phase

The ground state is the SM phase when $|\lambda_r - \lambda_{cr}| > \lambda^C$ and $\lambda_r\lambda_{cr} < 0$. The SM phase has two sets of imaginary-number displacements $(\alpha, \beta) = \pm(i\alpha_0, i\beta_0)$ with

$$\alpha_0 = -(\lambda_r - \lambda_{cr})\sqrt{N\left(1-\mu_M^2\right)}/2\tilde{\omega}_c, \tag{B10a}$$

$$\beta_0 = \sqrt{N(1-\mu_M)/2}, \tag{B10b}$$

where $\mu_M = [\lambda^C/(\lambda_r - \lambda_{cr})]^2$. The corresponding second-order Hamiltonian can be obtained as

$$\begin{aligned} H_{\rm rot}^{(2)} =& \tilde{\omega}_0\frac{1+\mu_M}{2\mu_M}d^\dagger d + \tilde{\omega}_c c^\dagger c \\ &+ \frac{\lambda_r+\lambda_{cr}}{2}\sqrt{\frac{1+\mu_M}{2}}(c+c^\dagger)(d^\dagger+d) \\ &+ \frac{\mu_M(\lambda_r-\lambda_{cr})}{\sqrt{2(1+\mu_M)}}(c-c^\dagger)(d^\dagger-d) \\ &- \tilde{\omega}_0\frac{(3+\mu_M)(1-\mu_M)}{8\mu_M(1+\mu_M)}(d^\dagger-d)^2 + E_G. \end{aligned} \tag{B11}$$

c. SEMa phase

For $\lambda_r = 0$ (i.e., only with nonzero counter-rotating terms) and when $|\lambda_{cr}| > \lambda^C$, the system is in the SEMa phase with the semiclassical displacements $(\alpha, \beta) = (\alpha_0 e^{-i\theta}, \beta_0 e^{i\theta})$, where $\alpha_0 = -\lambda_{cr}\sqrt{N(1-\mu_{\rm E}^2)}/2\tilde{\omega}_c$ and $\beta_0 = \sqrt{N(1-\mu_E)/2}$. In these solutions, the displacements of the operators a and b carry an opposite phase factor $\mp\theta$, which can be an arbitrary angle. The corresponding second-order Hamiltonian can be obtained as

$$\begin{aligned} H_{\rm rot}^{(2)} =& \tilde{\omega}_0\frac{1+\mu}{2\mu}d^\dagger d + \tilde{\omega}_c c^\dagger c \\ &+ \frac{(\lambda_r+\lambda_{cr})(1+3\mu)}{2\sqrt{2(1+\mu)}}(c^\dagger d^\dagger + cd) \\ &- \frac{(\lambda_r+\lambda_{cr})(1-\mu)}{2\sqrt{2(1+\mu)}}(e^{2i\theta}cd^\dagger + e^{-2i\theta}c^\dagger d) \\ &+ \tilde{\omega}_0\frac{(1-\mu)}{8\mu}\frac{(3+\mu)}{(1+\mu)}(e^{i\theta}d^\dagger + e^{-i\theta}d)^2 + E_G. \end{aligned} \tag{B12}$$

Note that in this case $\mu_M = \mu_E = \tilde{\omega}_0\tilde{\omega}_c/\lambda_{cr}^2 = \mu$.

d. SEMb phase

For $\lambda_{cr} = 0$ (i.e., only with nonzero rotating terms) and when $|\lambda_r| > \lambda^C$, the system is in the superradiant electromagnetic b (SEMb) phase with the semiclassical displacements $(\alpha, \beta) = (\alpha_0 e^{i\theta}, \beta_0 e^{i\theta})$, where $\alpha_0 = -\lambda_r\sqrt{N(1-\mu_E^2)}/2\tilde{\omega}_c$ and β_0 is the same as defined above in the SEMa phase. In these solutions, the displacements of the operators a and b carry an arbitrary but equal phase factor θ. The corresponding second-order Hamiltonian can be obtained as

$$\begin{aligned} H_{\rm rot}^{(2)} =& \tilde{\omega}_0\frac{1+\mu'}{2\mu'}d^\dagger d + \tilde{\omega}_c c^\dagger c \\ &+ \frac{(\lambda_r+\lambda_{cr})(1+3\mu')}{2\sqrt{2(1+\mu')}}(cd^\dagger + c^\dagger d) \\ &- \frac{(\lambda_r+\lambda_{cr})(1-\mu')}{2\sqrt{2(1+\mu')}}(e^{-2i\theta}cd + e^{2i\theta}c^\dagger d^\dagger) \\ &+ \tilde{\omega}_0\frac{(1-\mu')(3+\mu')}{8\mu'(1+\mu')}(e^{i\theta}d^\dagger + e^{-i\theta}d)^2 + E_G. \end{aligned} \tag{B13}$$

Here $\mu_M = \mu_E = \tilde{\omega}_0\tilde{\omega}_c/\lambda_r^2 = \mu'$.

e. Symmetry

The SE and SM phases have two sets of solutions $(\pm\alpha, \pm\beta)$. In the SE and SM regions of the phase diagram with $\lambda_r\lambda_{cr} \neq 0$, the Hamiltonian has Z_2 symmetry. The solutions are Z_2 symmetry-breaking states of the Hamiltonian. Meanwhile, in the SEMa and SEMb regions with $\lambda_r\lambda_{cr} = 0$, the Hamiltonian has U(1) symmetry. The solutions are U(1) symmetry-breaking states with an arbitrary phase θ. The U(1) symmetry of the Hamiltonian results in a Goldstone quasiparticle mode with zero frequency, as will be shown in Appendix C.

APPENDIX C: QUASIPARTICLE MODES

In this section, we diagonalize the Hamiltonian $H_{\rm rot}^{(2)}$ using the Hopfield-Bogoliubov transformation [37] and derive the quasiparticle modes in the normal and superradiant phases, respectively. The Hamiltonian $H_{\rm rot}^{(2)}$ can be diagonalized as

$$H_{\rm rot}^{(2)} = \sum_{i=\pm}\omega_i^p\gamma_i^{p\dagger}\gamma_i^p + E_G^p, \tag{C1}$$

where p =N, SE, SM, SEMa, and SEMb refers to the phase of the ground state, γ_i^p ($\gamma_i^{p\dagger}$) is the annihilation (creation) operator of the quasiparticle mode with frequency ω_i^p, and $[\gamma_i^p, \gamma_j^{p\dagger}] = \delta_{i,j}$. There are two quasiparticle modes $\pm$ in each phase. The operators of the quasiparticle modes can be expressed as

$$\gamma_i^p = \vec{h}_{ip}^T\vec{v}_S, \tag{C2}$$

where $\vec{v}_S = (a, b, a^\dagger, b^\dagger)^T$ for the normal phase with $\alpha = \beta = 0$ and $\vec{v}_S = (c, d, c^\dagger, d^\dagger)^T$ for the superradiant phase, and $\vec{h}_{ip}$ is a 4×1 vector that gives the coefficient for the operator component of the corresponding mode.

The coefficient vectors $\vec{h}_{ip} = (h_{i,1}^p, h_{i,2}^p, h_{i,3}^p, h_{i,4}^p)^T$ for the quasiparticle mode γ_i^p in phase p can be solved from the eigenvectors of the Bogoliubov matrix

$$M_p^T = \begin{pmatrix} \tilde{\omega}_c & \widetilde{\Omega}_c^* & 0 & \widetilde{\Omega}_d \\ \widetilde{\Omega}_c & \tilde{\omega}_0' & \widetilde{\Omega}_d & D \\ 0 & -\widetilde{\Omega}_d^* & -\tilde{\omega}_c & -\widetilde{\Omega}_c \\ -\widetilde{\Omega}_d^* & -D^* & -\widetilde{\Omega}_c^* & -\tilde{\omega}_0' \end{pmatrix}. \tag{C3}$$

Here the superscript "T" in the expression M_p^T denotes the transpose operation on the matrix M_p. The matrix M_p is obtained by deriving the Heisenberg equations for the operators in $\vec{v}_S$ using the Hamiltonian $H_{\rm rot}^{(2)}$. In Table I, we give the expressions for $\tilde{\omega}_0'$, $\widetilde{\Omega}_c$, $\widetilde{\Omega}_d$, and D in the matrix M_p^T for all phases p.

TABLE I. The parameters $\widetilde{\omega}_0'$, $\widetilde{\Omega}_c$, $\widetilde{\Omega}_d$, and D for all phases.

	N	SE	SM	SEMa	SEMb
$\widetilde{\omega}_0'$	$\tilde{\omega}_0$	$\tilde{\omega}_0\frac{1+\mu_E}{2\mu_E}+w_3\,\tilde{\omega}_0\frac{1+\mu_M}{2\mu_M}-v_3\,\tilde{\omega}_0\frac{1+\mu}{2\mu}+s_0(\mu)\,\tilde{\omega}_0\frac{1+\mu'}{2\mu'}+s_0(\mu')$			
$\widetilde{\Omega}_c$	λ_r	w_1	v_1	$s_1(\mu)$	$-s_2(\mu')$
$\widetilde{\Omega}_d$	$-\lambda_{cr}$	w_2	v_2	$s_2(\mu)$	$-s_1(\mu')$
D	0	$-w_3$	$-v_3$	$-s_0(\mu)e^{-2i\theta}$	$-s_0(\mu')e^{-2i\theta}$

The expressions of w_j, v_j, s_j $(j=1,2,3)$ in Table I are given by

$$w_1=\Omega_M\sqrt{\frac{1+\mu_E}{2}}+\Omega_E\mu_E\sqrt{\frac{2}{1+\mu_E}}, \tag{C4a}$$

$$w_2=\Omega_M\sqrt{\frac{1+\mu_E}{2}}-\Omega_E\mu_E\sqrt{\frac{2}{1+\mu_E}}, \tag{C4b}$$

$$w_3=\tilde{\omega}_0\frac{(1-\mu_E)}{(1+\mu_E)}\frac{(3+\mu_E)}{4\mu_E}, \tag{C4c}$$

$$v_1=\Omega_M\mu_M\sqrt{\frac{2}{1+\mu_M}}+\Omega_E\sqrt{\frac{1+\mu_M}{2}}, \tag{C5a}$$

$$v_2=\Omega_M\mu_M\sqrt{\frac{2}{1+\mu_M}}-\Omega_E\sqrt{\frac{1+\mu_M}{2}}, \tag{C5b}$$

$$v_3=-\tilde{\omega}_0\frac{(3+\mu_M)(1-\mu_M)}{4\mu_M(1+\mu_M)}, \tag{C5c}$$

and

$$s_0(\mu)=\tilde{\omega}_0\frac{(1-\mu)}{4\mu}\frac{(3+\mu)}{(1+\mu)}, \tag{C6a}$$

$$s_1(\mu)=-\Omega_E\frac{(1-\mu)}{\sqrt{2(1+\mu)}}e^{-2i\theta}, \tag{C6b}$$

$$s_2(\mu)=-\Omega_E\frac{(1+3\mu)}{\sqrt{2(1+\mu)}}, \tag{C6c}$$

where

$$\Omega_E=\frac{\lambda_r+\lambda_{cr}}{2}, \tag{C7a}$$

$$\Omega_M=\frac{\lambda_r-\lambda_{cr}}{2}. \tag{C7b}$$

The Bogoliubov matrix M_p^T has four eigenvalues: $\pm\omega_+^p$, $\pm\omega_-^p$, among which $\omega_+^p,\omega_-^p\geqslant 0$ are the two quasiparticle frequencies. We derive that

$$\omega_\pm^p=\frac{\sqrt{Y\pm\sqrt{X}}}{\sqrt{2}}, \tag{C8}$$

where

$$Y=\zeta^2+8\upsilon\chi+\tilde{\omega}_c^2, \tag{C9}$$

$$X=16(\zeta\chi+\upsilon\tilde{\omega}_c)(\zeta\upsilon+\chi\tilde{\omega}_c)+\left(\zeta^2-\tilde{\omega}_c^2\right)^2, \tag{C10}$$

and the expressions of υ, χ, and ζ for all phases are given in Table II.

TABLE II. The parameters (υ,χ,ζ) for all phases.

	N	SE	SM	SEMa	SEMb
υ	Ω_E	$\mu_E\Omega_E$	Ω_E	$\mu\Omega_E$	$\mu'\Omega_E$
χ	Ω_M	Ω_M	$\mu_M\Omega_M$	$-\Omega_E$	Ω_E
ζ	$\tilde{\omega}_0$	$\frac{\tilde{\omega}_0}{\mu_E}$	$\frac{\tilde{\omega}_0}{\mu_M}$	$\frac{\tilde{\omega}_0}{\mu}$	$\frac{\tilde{\omega}_0}{\mu'}$

With the above result, the quasiparticle frequencies in the normal phase can be derived as

$$\omega_\pm^N=\frac{1}{\sqrt{2}}\Big\{-2\lambda_{cr}^2+2\lambda_r^2+\tilde{\omega}_0^2+\tilde{\omega}_c^2 \pm\sqrt{\left[4\lambda_r^2+(\tilde{\omega}_0-\tilde{\omega}_c)^2\right](\tilde{\omega}_0+\tilde{\omega}_c)^2-4\lambda_{cr}^2(\tilde{\omega}_0-\tilde{\omega}_c)^2}\Big\}^{1/2}. \tag{C11}$$

Within the parameter region of the normal phase as labeled in Fig. 2 of the main paper, both ω_+ and ω_- are real numbers, which is consistent with our discussion of the phase diagram. For the SEMa and SEMb phases, we find that

$$\omega_-^{\mathrm{SEMa}}=\omega_-^{\mathrm{SEMb}}=0, \tag{C12}$$

which describes a Goldstone mode due to the U(1) symmetry of the Hamiltonian when either λ_r or λ_{cr} equals to zero. We also find that in the SEMa phase,

$$\omega_+^{\mathrm{SEMa}}=\sqrt{\frac{\lambda_{cr}^4}{\tilde{\omega}_c^2}+\tilde{\omega}_c(-2\tilde{\omega}_0+\tilde{\omega}_c)}, \tag{C13}$$

and in the SEMb phase,

$$\omega_+^{\mathrm{SEMb}}=\sqrt{\frac{\lambda_r^4}{\tilde{\omega}_c^2}+\tilde{\omega}_c(2\tilde{\omega}_0+\tilde{\omega}_c)}. \tag{C14}$$

We plot the excitation spectrum $\omega_\pm$ for all parameter regions in Fig. 6 vs the effective couplings λ_r and λ_{cr} at $\upsilon/\omega_0=0.49$ for $g_0/\omega_0=0.06$ and $\omega_0=\omega_c'$. The superscript "p" that refers to the specific phase in the quasiparticle frequency is omitted. The phase boundaries are indicated by the white lines.

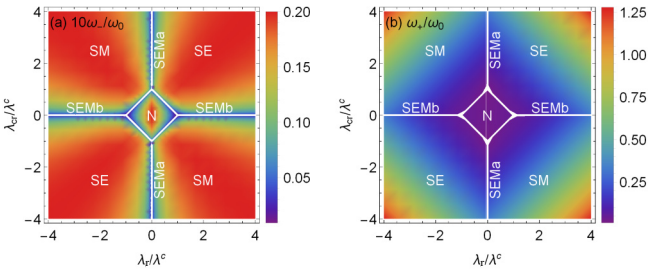

FIG. 6. The relative quasiparticle spectrum (a) $10\omega_-/\omega_0$ and (b) ω_+/ω_0 given by Eq. (C8) vs λ_r/λ^C and λ_{cr}/λ^C for $\upsilon/\omega_0=0.49$. The superscript "p" for a specific phase in the quasiparticle frequency is omitted. Other parameters are $g_0/\omega_0=0.06$, and we choose $\omega_0=\omega_c'=1$ as the energy unit.

[1] R. H. Dicke, Coherence in spontaneous radiation processes, Phys. Rev. **93**, 99 (1954).

[2] F. Dimer, B. Estienne, A. S. Parkins, and H. J. Carmichael, Proposed realization of the Dicke-model quantum phase transition in an optical cavity QED system, Phys. Rev. A **75**, 013804 (2007).

[3] K. Baumann, C. Guerlin, F. Brennecke, and T. Esslinger, Dicke quantum phase transition with a superfluid gas in an optical cavity, Nature (London) **464**, 1301 (2010).

[4] D. Nagy, G. Kónya, G. Szirmai, and P. Domokos, Dicke-Model Phase Transition in the Quantum Motion of a Bose-Einstein Condensate in an Optical Cavity, Phys. Rev. Lett. **104**, 130401 (2010).

[5] K. Baumann, R. Mottl, F. Brennecke, and T. Esslinger, Exploring Symmetry Breaking at the Dicke Quantum Phase Transition, Phys. Rev. Lett. **107**, 140402 (2011).

[6] J. M. Fink, R. Bianchetti, M. Baur, M. Göppl, L. Steffen, S. Filipp, P. J. Leek, A. Blais, and A. Wallraff, Dressed Collective Qubit States and the Tavis-Cummings Model in Circuit QED, Phys. Rev. Lett. **103**, 083601 (2009).

[7] P. Macha, G. Oelsner, J.-M. Reiner, M. Marthaler, S. André, G. Schön, U. Hübner, H.-G. Meyer, E. Il'ichev, and A. V. Ustinov, Implementation of a quantum metamaterial using superconducting qubits, Nat. Commun. **5**, 5146 (2014).

[8] C. Emary and T. Brandes, Quantum Chaos Triggered by Precursors of a Quantum Phase Transition: The Dicke Model, Phys. Rev. Lett. **90**, 044101 (2003).

[9] C. Emary and T. Brandes, Chaos and the quantum phase transition in the Dicke model, Phys. Rev. E **67**, 066203 (2003).

[10] A. Baksic and C. Ciuti, Controlling Discrete and Continuous Symmetries in "Superradiant" Phase Transitions with Circuit QED Systems, Phys. Rev. Lett. **112**, 173601 (2014).

[11] M. Soriente, T. Donner, R. Chitra, and O. Zilberberg, Dissipation-Induced Anomalous Multicritical Phenomena, Phys. Rev. Lett. **120**, 183603 (2018).

[12] S. Sachdev, *Quantum Phase Transition* (Cambridge University Press, Cambridge, 1999).

[13] J.-F. Huang, Y. Li, J.-Q. Liao, L.-M. Kuang, and C. P. Sun, Dynamic sensitivity of photon-dressed atomic ensemble with quantum criticality, Phys. Rev. A **80**, 063829 (2009).

[14] K. Hepp and E. H. Lieb, On the superradiant phase transition for molecules in a quantized radiation field: The Dicke maser model, Ann. Phys. (NY) **76**, 360 (1973).

[15] Y. K. Wang and F. T. Hioe, Phase transition in the Dicke model of superradiance, Phys. Rev. A **7**, 831 (1973).

[16] M. J. Bhaseen, J. Mayoh, B. D. Simons, and J. Keeling, Dynamics of nonequilibrium Dicke models, Phys. Rev. A **85**, 013817 (2012).

[17] V. Link and W. T. Strunz, Dynamical Phase Transitions in Dissipative Quantum Dynamics with Quantum Optical Realization, Phys. Rev. Lett. **125**, 143602 (2020).

[18] R. J. Lewis-Swan, S. R. Muleady, D. Barberena, J. J. Bollinger, and A. M. Rey, Characterizing the dynamical phase diagram of the Dicke model via classical and quantum probes, Phys. Rev. Res. **3**, L022020 (2021).

[19] M. Kulkarni, B. Öztop, and H. E. Türeci, Cavity-Mediated Near-Critical Dissipative Dynamics of a Driven Condensate, Phys. Rev. Lett. **111**, 220408 (2013).

[20] J. A. Muniz, D. Barberena, R. J. Lewis-Swan, D. J. Young, J. R. K. Cline, A. M. Rey, and J. K. Thompson, Exploring dynamical phase transitions with cold atoms in an optical cavity, Nature (London) **580**, 602 (2020).

[21] J. Klinder, H. Keßler, M. Wolke, L. Mathey, and A. Hemmerich, Dynamical phase transition in the open Dicke model, Proc. Natl. Acad. Sci. USA **112**, 3290 (2015).

[22] H. Ritsch, P. Domokos, F. Brennecke, and T. Esslinger, Cold atoms in cavity-generated dynamical optical potentials, Rev. Mod. Phys. **85**, 553 (2013).

[23] Z. Zhang, C. H. Lee, R. Kumar, K. J. Arnold, S. J. Masson, A. S. Parkins, and M. D. Barrett, Nonequilibrium phase transition in a spin-1 Dicke model, Optica **4**, 424 (2017).

[24] Z. Zhang, C. H. Lee, R. Kumar, K. J. Arnold, S. J. Masson, A. L. Grimsmo, A. S. Parkins, and M. D. Barrett, Dicke-model simulation via cavity-assisted Raman transitions, Phys. Rev. A **97**, 043858 (2018).

[25] K. Rzażewski, K. Wódkiewicz, and W. Żakowicz, Phase Transitions, Two-Level Atoms, and the A^2 Term, Phys. Rev. Lett. **35**, 432 (1975).

[26] P. Nataf and C. Ciuti, No-go theorem for superradiant quantum phase transitions in cavity QED and counter example in circuit QED, Nat. Commun. **1**, 72 (2010).

[27] T. Niemczyk, F. Deppe, H. Huebl, E. P. Menzel, F. Hocke, M. J. Schwarz, J. J. García-Ripoll, D. Zueco, T. Hümmer, E. Solano, A. Marx, and R. Gross, Circuit quantum electrodynamics in the ultrastrong-coupling regime, Nat. Phys. **6**, 772 (2010).

[28] P. Forn-Díaz, J. Lisenfeld, D. Marcos, J. J. García-Ripoll, E. Solano, C. J. P. M. Harmans, and J. E. Mooij, Observation of the Bloch-Siegert Shift in a Qubit-Oscillator System in the Ultrastrong Coupling Regime, Phys. Rev. Lett. **105**, 237001 (2010).

[29] F. Yoshihara, T. Fuse, S. Ashhab, K. Kakuyanagi, S. Saito, and K. Semba, Superconducting qubit-oscillator circuit beyond the ultrastrong-coupling regime, Nat. Phys. **13**, 44 (2017).

[30] P. Forn-Díaz, J. J. García-Ripoll, B. Peropadre, J.-L. Orgiazzi, M. A. Yurtalan, R. Belyansky, C. M. Wilson, and A. Lupascu, Ultrastrong coupling of a single artificial atom to an electromagnetic continuum in the nonperturbative regime, Nat. Phys. **13**, 39 (2017).

[31] S. J. Bosman, M. F. Gely, V. Singh, A. Bruno, D. Bothner, and G. A. Steele, Multi-mode ultra-strong coupling in circuit quantum electrodynamics, npj Quantum Inf. **3**, 46 (2017).

[32] S. Ashhab and K. Semba, Superradiance phase transition in the presence of parameter fluctuations, Phys. Rev. A **95**, 053833 (2017).

[33] M. Tavis and F. W. Cummings, Exact solution for an N-molecule-radiation-field Hamiltonian, Phys. Rev. **170**, 379 (1968).

[34] H. J. Lipkin, N. Meshkov, and A. J. Glick, Validity of many-body approximation methods for a solvable model: (I). Exact solutions and perturbation theory, Nucl. Phys. **62**, 188 (1965); N. Meshkov, A. J. Glick, and H. J. Lipkin, Validity of many-body approximation methods for a solvable model: (II). Linearization procedures, *ibid.* **62**, 199 (1965); A. J. Glick, H. J. Lipkin, and N. Meshkov, Validity of many-body approximation methods for a solvable model: (III). Diagram summations, *ibid.* **62**, 211 (1965).

[35] J.-F. Huang, J.-Q. Liao, L. Tian, and L.-M. Kuang, Manipulating counter-rotating interactions in the quantum Rabi model via modulation of the transition frequency of the two-level system, Phys. Rev. A **96**, 043849 (2017).

[36] T. Holstein and H. Primakoff, Field dependence of the intrinsic domain magnetization of a ferromagnet, Phys. Rev. **58**, 1098 (1940).

[37] J. J. Hopfield, Theory of the contribution of excitons to the complex dielectric constant of crystals, Phys. Rev. **112**, 1555 (1958).

[38] M. Kjaergaar, M. E. Schwartz, J. Braumüller, P. Krantz, J. I.-J. Wang, S. Gustavsson, and W. D. Oliver, Superconducting qubits: Current state of play, Annu. Rev. Condens. Matter Phys. **11**, 369 (2020).

[39] A. Blais, R.-S. Huang, A. Wallraff, S. M. Girvin, and R. J. Schoelkopf, Cavity quantum electrodynamics for superconducting electrical circuits: An architecture for quantum computation, Phys. Rev. A **69**, 062320 (2004).

[40] K. Cai, P. Parajuli, G.-L. Long, C.-W. Wong, and L. Tian, Robust preparation of many-body ground states in Jaynes-Cummings lattices, npj Quantum Inf. **7**, 96 (2021).

[41] L. Tian, Cavity-assisted dynamical quantum phase transition at bifurcation points, Phys. Rev. A **93**, 043850 (2016).